LAWRENCE
LIVERMORE
NATIONAL
LABORATORY

LLNL-JRNL-844531

Multi-element isotopic analysis of hot particles from Chornobyl

D. van Eerten, M. Raiwa, P. Hanemann, L. Leifermann, T. Weissenborn, W. Schulz, M. Weiss, D. Z. Shulaker, P. Boone, D. G. Willingham, K. Thomas, B. Sammis, B. H. Isselhardt, M. R. Savina, C. Walther

January 30, 2023

Journal of Hazardous Materials

Disclaimer

Multi-element isotopic analysis of hot particles from Chornobyl

Darcy van Eerten[1], Manuel Raiwa[1], Paul Hanemann[1], Laura Leifermann[1], Tobias Weissenborn[1], Wolfgang Schulz[1], Martin Weiß[1], Danielle Ziva Shulaker[2], Peter Boone[2], David Willingham[2], Keenan Thomas[2], Brian Sammis[2], Brett Isselhardt[2], Mike Savina[2], and Clemens Walther[1]

[1]Institut für Radioökologie und Strahlenschutz, Leibniz Universität Hannover, Herrenhäuser Str. 2, 30419 Hannover, Germany.
[2]Chemical and Isotopic Signatures Group, Lawrence Livermore National Laboratory, Livermore, USA.

February 2023

Abstract

Microscopic fuel fragments, so-called "hot particles", were released during the 1986 accident at the Chornobyl nuclear powerplant and continue to contaminate the exclusion zone in northern Ukraine. Isotopic analysis can provide vital information about sample origin, history and contamination of the environment, though it has been underutilized due to the destructive nature of most mass spectrometric techniques, and inability to remove isobaric interference. Recent developments have diversified the range of elements that can be investigated through resonance ionization mass spectrometry (RIMS), notably in the fission products. The purpose of this study is to demonstrate the application of multi-element analysis on hot particles as relates to their burnup, particle formation in the accident, and weathering. The particles were analysed with two RIMS instruments: resonant-laser secondary neutral mass spectrometry (rL-SNMS) at the Institute for Radiation Protection and Radioecology (IRS) in Hannover, Germany, and laser ionization of neutrals (LION) at Lawrence Livermore National Laboratory (LLNL) in Livermore, USA. Comparable results across instruments show a range of burnup dependent isotope ratios for U and Pu and Cs, characteristic of RBMK-type reactors. Results for Rb, Ba and Sr show the influence of the environment, retention of Cs in the particles and time passed since fuel discharge.

Keywords— RIMS, actinides, fission products, ultra-trace analysis

1 Introduction

Characterizing the hazards posed by nuclear material in the environment is important in both the immediate response to a contamination event and its subsequent long-term management. So-called "hot particles" are derived from nuclear material, typically in the size range of μm. Much of what we know about these particles is based on context; where and when the contamination took place. This work looks directly at individual hot particles from the perspective of the nuclear reactions that produced them, and investigates how rapid isotope ratio analysis can non-destructively answer questions relevant to radioecology and nuclear forensics. Previous work has demonstrated how the resonant laser secondary neutral mass spectrometry (rL-SNMS) instrument in Hannover, Germany can measure isotope ratios in the actinides U, Pu and Am on hot particles from the Chornobyl Exclusion Zone (CEZ) [1, 2]. Here, this capability is extended to the fission products Cs, Rb, Sr and Ba by use of the laser ionization of neutrals (LION) instrument in Livermore, USA [3].

The 1986 accident at the Chornobyl nuclear powerplant (ChNPP) deposited a vast number of hot particles in the 30 km exclusion zone that remain there to this day [4, 5]. These particles are fuel fragments originating from the reactor core, and are composed of a large variety of stable and radioactive nuclides [6, 7]. They not only pose a radiological risk via inhalation [8], but will also weather and degrade over time, leaching radionuclides into the environment [7].

As noted by Konings et al., the material properties of emitted nuclear material will be affected on the microscale by reactor operation, and on the macro scale by the conditions of the accident scenario [9]. Kashparov and Salbu et al. have focused on the latter by categorizing particle morphology on the distinct phases of the accident: those physically ejected in the first explosions, and those highly chemically altered by the graphite fires in the following days. The most chemically stable are particles that fused with the zircalloy cladding at high temperatures, while chemically low stable particles were highly oxidized [10, 11, 7]. This work considers those attributes in relation to the reactor-derived isotopic composition of the individual particles, with emphasis on the fission products and how those were affected by the accident and subsequent weathering.

1.1 Hot Particle Analysis

Scanning (tunneling) electron microscopy SEM (or STEM), combined with density information provided by back-scattered electrons (BSE), are the primary methods of imaging hot particles and characterizing their surface morphology [12, 13, 7]. Energy dispersive X-ray spectroscopy (EDS) can be combined with these techniques to identify major components of a particle. This is how U-Zr fused particles can be identified in the CEZ [7], or U-Nb particles can be found in Dounreay [14]. In particles from Fukushima, highly concentrated Cs and other fissionogenic elements can be identified by EDS [12]. The sensitivity of EDS however is limited, which means minor elements such as Pu or even Cs can remain unidentified.

For a more sensitive and quantitative element map, micro or nano X-ray flourescence (XRF) can be used [13, 12]. Such methods are powerful tools for measuring very small or heterogenous particles, but lack essential isotopic information. For example, they cannot distinguish between natural and enriched uranium.

Nuclear forensics has long used isotope ratios to determine the origin and history of unknown nuclear material [15, 16, 17]. Actinide ratios serve as characteristic fingerprints of reactor design and operation [18, 19], as do fission products [20, 21]. Measuring these ratios typically involves a tailored approach for each element through a combination of radiometric and mass spectrometric techniques, some of which are destructive.

Radiometric techniques such as gamma and alpha spectrometry are non-destructive and regularly used to determine isotope ratios on bulk samples such as fuel pellets [22]. For microscopic particles, such analyses are time-consuming and often limited to the highest activity radioisotopes such as ^{137}Cs and ^{241}Am. Short-lived isotopes such as ^{134}Cs (half-life 2.1 years) can only be measured shortly after an accident [12]. Beta-only emitters such as ^{90}Sr require long measurement times in combination with chemical preparation [23], and has been measured in limited capacity in hot particles [14].

Mass spectrometry enables ultra-trace analysis for both active and inactive isotopes. Though highly sensitive, inductively couple plasma (ICP-MS) requires the sacrifice (dissolution) of a hot particle for analysis [13], and may require extensive chemical preparation to remove environmental and isobaric interference [21]. Secondary ion mass spectrometry (SIMS), allows spatially resolved measurement of a solid sample (less than EDS, but far more sensitive). Nano-SIMS boasts higher spatial resolution [24], and large sector SIMS instruments achieve higher mass resolution [12]. However, neither technique removes enviromental or isobaric interferences completely, as shown by Morooka et al. in their analysis of ^{135}Cs/^{137}Cs isotope ratios in Fukushima particles, which are hampered by ^{135}Ba and ^{137}Ba [12]. Hydride formation presents another challenge, which depends on sample matrix and analysis method. As noted by Fallon et al. in the analysis of a single enriched fuel particle, ^{238}U^{1}H formed ca. 0.55 % of the ^{238}U, used to show the insignificant interference on ^{235}U by ^{234}U^{1}H [24]. This is however not insignificant when measuring the ^{236}U produced through irradiation, or any of the ^{239,240,241,242}Pu isotopes. In short, such techniques focus on one element or isotope ratio at a time.

Resonant laser ionization adds the necessary selectivity, targeting the electronic structure of a given element to step-wise excite it beyond the ionization potential [25, 26, 27]. The technique removes the need for chemical preparation, which allows for multiple analyses to take place on the same sample. Resonance ionization mass spectrometry (RIMS) requires only a suitable mass spectrometer, an efficient excitation scheme per element [28], and the lasers to produce the necessary wavelengths [29]. These requirements are not trivial, making RIMS facilities rare in the world. Its true strength lies in its range and speed, as advances in both laser design and ionization schemes have broadened the scope of elements that can be investigated.

The work presented here leverages the specializations of two different RIMS instruments to investigate a diverse range of isotopes in CEZ hot particles. Both the rL-SNMS facility [30, 1] and the LION facility [31, 3] are non-destructive RIMS techniques based on the principles of time-of-flight secondary ion mass spectrometry (ToF-SIMS), making them suitable for surface analysis. The secondary ion fraction is removed, while the neutral fraction is ionized by the lasers. rL-SNMS is spatially resolved, giving a direct analysis of the isotope distribution on the surface of a sample. It can resonantly investigate one element at a time, and non-resonantly measure its oxides (as in [24]). LION is more sensitive, and can measure multiple elements simultaneously. However, to explore the applications of multi-element isotope ratio analysis one must understand the origin of their production.

1.2 Isotope production pathways

ChNPP was an RBMK-type Soviet reactor operating on low-enriched fuel with 2% ^{235}U [32, 33]. Though a total inventory of radionuclides in the ChNPP core has been estimated [34], the ratios vary considerably within the reactor itself, as shown both in models [35, 36] and by experiments [37, 38]. For every isotope, multiple production paths may be posssible, turning each ratio into a unique indicator of radiation conditions. Within the reactor, these various ratios are dependent on initial composition, neutron energy and flux. Once out of the reactor, other factors become dominant, namely chemical behaviour and time.

Even from a microscopic fuel particle, a surprisingly comprehensive characterisation can be made by targeting a range of isotopes, both in the actinides and fission products. As fuel burns up, the isotopic composition changes, serving as a characteristic fingerprint of the design and operation history of the reactor [19, 17]. Burnup quantifies the energy produced in the reactor normalized by its fuel load, typically expressed in MWd/kgU. It scales with the number of fissions that have occurred per unit mass of fuel. Burnup is therefore a proxy for the neutron fluence that drives transuranic isotope production and alters the composition of most fission products by neutron capture after they are produced. By comparing isotope ratios to burnup, we can assess the influences inside and outside the reactor.

1.2.1 Actinides

^{235}U/^{238}U decreases with burnup, due to fission or through neutron capture to produce ^{236}U and ^{239}Pu respectively. ^{236}U/^{238}U, ^{240}Pu/^{239}Pu, ^{241}Pu/^{239}Pu increase linearly with burnup, while ^{242}Pu/^{239}Pu increases at an accelerated rate [37]. The rate of increase can distinguish RBMKs from other reactors such as WWERs (Soviet light water reactors), the only type to operate in Ukraine today [39].

Extensive chemical separation is typically utilized to isolate elements or isotopes of interest for analysis by radiometric or mass spectrometry techniques [37]. Separating the isobars ^{241}Am/^{241}Pu and ^{238}Pu/^{238}U are particularly challenging [38]. The former is easily resolved with laser ionization, while the latter is far more challenging due to its extremely low ratio down to 10^{-6} [29, 1, 3].

^{241}Am grows in over decades as ^{241}Pu decays, while ^{243}Am is produced almost exclusively during reactor operation. This presents an opportunity to observe the chemical behaviour of both plutonium and americium through the weathering of particles in the environment. If some plutonium, or recently produced americium should leach out of the particle, this could be reflected in lower ^{241}Am/^{243}Am ratios. This ratio in hot particles was briefly explored in previous work by [1], but did not show significant deviation from known RBMK ratios. Following this line of reasoning however, we can target other

isotopes that are dependent on the chemical behaviour of their precursors.

1.2.2 Fission Products

Fission produces a wide variety of isotopes. However, ^{137}Cs and ^{90}Sr are particularly consequential for humans and the environment [40, 23, 41]. These predominantly neutron-rich fission products quickly beta-decay until they reach a long-lived or stable isotope. On an elemental level, the fission product decay chains go from I $\rightarrow$ Xe $\rightarrow$ Cs $\rightarrow$ Ba, and Br $\rightarrow$ Kr $\rightarrow$ Rb $\rightarrow$ Sr. For nuclides that decay beyond reactor operation, the decay products become sensitive to the environment and time-frame. The accident at Chornobyl is particularly interesting in two time frames: the sudden cessation of reactor activity caused by the melt-down and explosion, and the environmental factors in the decades since.

The variables that contribute to the isotope ratios (fission, neutron capture, time) can be examined from first principles by looking at independent and cumulutive fission yields. These depend on the fissioning isotope and neutron energy, found in nuclear data libraries such as JEFF, JENDL, and ENDF [42]. Such ratios can be more accurately modeled by models such as web-KORIGEN++ [42], and subsequently compared to literature data where available.

^{138}Ba (stable) and ^{137}Cs (half-life 30 years) are directly produced in the reactor at a similar rate, and have neglible neutron absorption cross-sections. Aside from the decay of ^{137}Cs, ^{137}Ba is also produced independently in the reactor, but at only 1 % the rate of ^{138}Ba. The stability of Cs in samples exposed to weathering could be investigated by measuring the ^{137}Ba/^{138}Ba ratio in comparison to the ideal case. Purely via the thermal ^{235}U fission yields (in JEFF 3.3 [42]), with no decay, a ratio between ^{137}Cs/^{138}Ba of $\frac{6.09}{6.68} = 0.91$ would be expected. This increases with burnup as ^{239}Pu builds up and contributes to fission. After 36 years of ^{137}Cs decay, this will result in a range of ^{137}Ba/^{138}Ba ratios from 0.51 to 0.61 depending on burnup.

Modelling with webKORIGEN++, predicts a ratio of 0.56 for 10 MWd/kg and 0.58 for 16 MWd/kg, the range of burnup found in the CEZ hot particles. As webKORIGEN++ does not have an RBMK reactor model, a boiling water reactor (BWR) model was used, which estimates the ^{239}Pu contribution to be higher than is likely in RBMKs [37]. As shown by Robel et al. [20], a stable ratio ^{137}Ba/^{138}Ba of 0.53 ± 0.02 was measured on 33 year-old spent fuel samples that had never been exposed to environmental conditions. Ratios substantially below this range could therefore indicate depletion of radiocesium, such that ingrowth of ^{137}Ba is slowed or entirely stopped.

The ^{137}Cs contamination of Europe after the Chornobyl accident [43] has driven the measurement of Cs ratios in environmental samples to distinguish between contaminating events such as nuclear weapons testing and the Fukushima accident [21], or even between reactors in Fukushima [12]. The production of stable ^{135}Cs is dependent on ^{135}I and ^{135}Xe, with have half-lives of 6.6 and 9.1 hours respectively. ^{135}Xe has an extremely large neutron capture cross-section of 2.7 Mb. With increased neutron flux, neutron capture into ^{136}Xe is favoured over decay into ^{135}Cs, driving the large range in ^{137}Cs/^{135}Cs ratios sensitive to start up and shut down of a reactor [20]. In fuel irradiated for the same time, burnup reflects the total neutron flux and energy, and ^{137}Cs/^{135}Cs increases as ^{135}Cs decreases [20].

The environmental factors affecting this intra-elemental ratio should be minimal, as even the effects of the significant power surge (only seconds in duration) before the reactor meltdown will be small in comparison to two years of regular reactor operation. However, the fission products would need to remain captured in the particles to be measured, which is not guaranteed due to the immense heat and pressure of the meltdown and explosion. The noble gases Xe and Kr are assumed in the literature to have escaped immediately during the explosion [34]. However, it is possible that such gases can remain trapped in spent nuclear fuel [44]. Iodine and Cs are less volatile, but can also dissipate (see [43]), and only Cs has multiple isotopes at long enough half-lives to measure today.

A change in isotope ratios from environmental factors might be visible in Rb. A ^{85}Rb/^{87}Rb ratio of 0.41 would be expected from thermal fission, which increases to 0.53 if all ^{85}Kr (half-life 10.8 years) were to have decayed fully. However, measuring the extent of Kr retention in Chornobyl hot particles would be challenging as both Rb isotopes are naturally occurring.

If the range in ^{137}Cs/^{135}Cs ratios are characteristic of major events [21], ^{90}Sr/^{88}Sr ratios can be used as a more specific chronometer to calculate the time elapsed since fuel discharge. ^{90}Sr has a similar half-life to ^{137}Cs of 29.8 years. It is of particular concern to the environment as a chemical homologue to calcium, thereby readily taken up in places where calcium accumulates, such as in bones [45]. ^{88}Sr and ^{90}Sr are both direct fission products, produced in near equal ratio by both ^{235}U and ^{239}Pu, with very low neutron absorption cross sections (0.024 b and 0.010 b respectively). The ratio is therefore in theory minimally sensitive to burnup. Assuming ^{90}Sr decays outside the reactor, this could serve as a measure of time since fuel discharge, since both isotopes behave chemically identically. The measured ratio m can be compared to the estimated fission yield fy, such that

$$time = \ln(\frac{^{90}Sr}{^{88}Sr}_{fy} \times \frac{^{88}Sr}{^{90}Sr}_{m}) \times \frac{28.91}{\ln(2)}. \quad (1)$$

Using the above fission yields and 36 years since the Chernobyl accident, we would expect a ratio for ^{90}Sr/^{88}Sr around 0.67. Using webKORIGEN++, a ratio of 0.69 is calculated, using slightly different fission yields in the JEFF-2.2 library. This increase suggests that burnup may contribute to the ratio in the form of neutron capture on the short-lived ^{89}Sr (half-life 50.6 days), though it's neutron cross section is low (0.42 b). An estimate of time passed since fuel discharge could therefore be made within the range of two years, accounting for the variation in fission yields, and assuming burnup is an insignificant factor. Measuring this ratio on the Chornobyl particles, where the time of release is very well known, could demonstrate whether this ratio is useful as a time stamp of the event.

2 Methods

2.1 Hot Particles

Drill cores, pond sendiments, and asphalt scrapings were sampled in the CEZ in 2014 and 2017 [46]. The method of isolation and extraction of the particles is described by Leifermann et al. [46], but is briefly described here. After sieving the sample, high density particles are separated from the remaining sample using a high density polytungstate solution. Particles are imaged and identified in a scanning electron microscope (SEM) in backscatter mode to contrast the particle from the surrounding matrix. Energy-dispersive X-ray spectroscopy (EDS) is used to confirm the particle

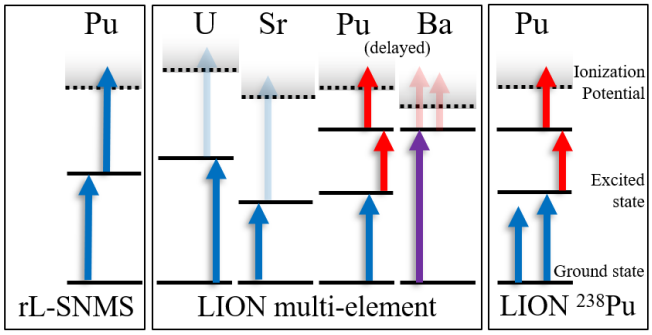

Figure 1: *Laser ionization schemes used in this work on rL-SNMS and LION to step-wise excite elements from the ground state to an autoinizing state beyond the ionization potential. Arrows indicate the laser wavelength and colour, transparent where lasers are being used in multiple schemes. The exact wavelengths for each step are given in the text where relevant or in the references [29, 48, 49]. For rL-SNMS two lasers were used. Six lasers were used in multi-element LION, with the Pu and Ba lasers delayed by one mass unit to remove interference by U and Cs respectively. Non-resonant ionization is used in the second steps for U, Sr and Ba. Four lasers were used for LION ^{238}Pu where the first step was blinked between resonant and non-resonant schemes.*

contains U, and Zr if applicable. Particles are then attached onto tungsten needles using SemGlu (Kleindiek Nanotechnik).

The selection of eight particles covers a range of burnups, morphologies and sampling location to study the impact on fission product ratios. The particles were reimaged at LLNL with an SEM (FEI, Inspect F model) at high vacuum with 5 kV current (Fig. 2). Gamma spectroscopy was performed at LLNL in coaxial and planar geometry. PeakEasy software [47] was used to determine the ratio between the count rate in counts per second (cps) on ^{241}Am (59 keV) and ^{137}Cs (661 keV) on the coax detector.

2.2 rL-SNMS

The rL-SNMS instrument in Hannover has been previously described in work by Raiwa [1]. The instrument consists of a time-of-flight mass spectrometer (TOFSIMS.5 by IONTOF), five Z-pinched 10 kHz Ti:Sa lasers (following the Mainz design [29]) pumped by three 532 nm Nd:YAG lasers. Two of these lasers were utlized for this study. A Bi^+ ion gun is used to sputter the first atomic layers of a sample, ionizing a fraction of the resulting atoms and molecules. In RIMS, the ionized fraction is removed by an external bias at +500 V, after which the lasers irradiate the remaining neutral fraction. The target element is ionized, along with oxidized forms of uranium and rare earth elements. In this study, U isotope ratios were measured simultaneously with resonance Pu by the non-resonant U oxides. A standard Pu solution was measured to correct for instrumental mass fractionation. Rastering the ion gun over the sample allows for a spatially resolved elemental intensity map at a beam size down to 70 nm, with the resolution achieved depending on the total ion signal available [41, 2]. For isotopes on the order of 10^2 counts per sample, 126 x 126 pixel raster size is chosen to balance signal intensity with spatial resolution.

2.3 LION

Livermore's LION instrument is similar to the rL-SNMS, but has a custom-built ToF-MS instrument [31]. We used an Nd:YAG laser at 1064 nm to desorb atoms and molecules from the surface. Because Rb and Cs are readily vaporized, they were were analyzed as secondary ions in which the signal was measured without resonantly ionizing the elements.

LION has six 1 kHz grating-tuned Ti:Sa lasers, pumped by three Nd:YLF lasers, with the possibility of lasing at fundamental, double, or triple frequency. Unlike the rL-SNMS, the lasers are not automated to switch between wavelengths. U, Sr, Pu and Ba were measured in the same spectrum, using a combination of ionization schemes (Fig. 1. Through use of a 200 ns delay, equivalent to 1 m/z [3], the U, Pu isobaric interference can be separated. Standards were measured to correct for isotopic mass fractionation.

$^{239-242}$Pu can be measured directly. Rather, ^{238}Pu is quantified by measuring the non-resonant contribution to the m/z 238 peak in a manner used previously on a Chornobyl hot particle [2]. In this work, an extra laser was tuned to be slightly off-resonance with the first step in the Pu scheme (figure 1, 420.864 nm), and alternated with the resonant laser (420.764 nm) such that every other shot was off-resonance. The off-resonance spectrum represents all sources of background and allows a quantitative correction. Alternating the on- and off-resonance lasers ensures that drifts in signal level over time do not affect the result. While it is possible to do this in a two-step scheme [1, 50], a three-step scheme is more successful at suppressing ^{238}U [2, 3].

2.4 Correction for environmental contamination

Environmental exposure can introduce natural ^{88}Sr, ^{137}Ba, and ^{138}Ba. The extent of contamination can be calculated using the non-fission isotopes of Sr and Ba. The two most abundant non-fission isotopes are used to estimate the natural fraction and averaged. In the example of Sr, these isotopes are ^{86}Sr and ^{87}Sr such that the estimated $^{88}Sr_e$ can be calculated as

$$^{88}Sr_e = \frac{1}{2} \times \left(\frac{^{86}Sr_m}{^{86}R} + \frac{^{87}Sr_m}{^{87}R}\right) \quad (2)$$

where ^{A}R is the ratio to ^{88}Sr as measured by isotopic standard, and $^{86}Sr_m$ and $^{87}Sr_m$ are the measured peaks. Errors are propagated by the sum of squares of relative errors on each measurement. The corrections for ^{137}Ba and ^{138}Ba are identical, using peaks on ^{135}Ba and ^{136}Ba. The total ratio subtracts this estimated contaminant, and must then be corrected for the fractionation caused by the lasers. This is significant in barium due to odd-isotope enhancement caused by hyperfine splitting [51]. The final ratio for barium is then

$$\frac{^{137}Ba}{^{138}Ba} = \frac{^{137}Ba_m - ^{137}Ba_e}{^{138}Ba_m - ^{138}Ba_e} \times \frac{K}{R}, \quad (3)$$

where K and R are the known ratio and standard measured ratios of ^{137}Ba/^{138}Ba. Further information on error analysis can be found in the supplementary materials.

3 Results and Discussion

3.1 SEM

The BSE results from the particles in fig. 2 show the diverse range of morphologies represented in a small sample set,

ranging in activity from 10^{-1} - 10^{2} Bq per particle. Following the categorization of Kashparov, the visual attributes of the particles could be indicative of their formation in the accident, and consequently relate to their rate of dissolution in the environment [7]. A full analysis of the reactivity with the environment would require a detailed analysis of the oxidation state, which requires X-ray spectroscopy techniques such as X-ray absorption near-edge structure (XANES), as studied for uranium in Dounreay particles [13] or extended X-ray absorption fine structure (EXAFS), as studied on Cs species in Fukushima [52]. Such analysis is beyond the scope of this study, however consideration of their morphology is a helpful classification tool for comparison with other studies [53, 46].

Kashparov's first category describes those which were ejected from the reactor during the explosion without significant chemical alteration or visual alteration to the UO_2 fuel's ceramic structure, and consequently a low environmental dissolution rate. Particle C036 (light orange) shows a very smooth particle surface compared to other particles. B018 (light green) shows a more laminated structure. B024 (violet) exhibits typical high burnup structure, characterized by the visible grain boundaries through which fission gases dissipate [9].

Kashparov's second category covers those highly oxidized by the high temperatures of the explosion and subsequent fires. C008 (yellow) and B022 (indigo) both showcase these highly porous forms. While B022 maintains a cubic structure, C008 has completely fractured, and is enveloped by organic material containing silicon (see supplementary for EDS results). Kashparov et al. identify these as the most susceptible to dissolution in the environment, though it should be noted that they were sampled long after their estimated dissolution half-life of 1-7 years [10]. B010 (bright orange) could also be featured in this category, as it has a similar aggregate form, though resolution is poor due to its small size and low conductivity. Though U is clearly identified in the EDS spectrum (see supplementary), no ^{137}Cs or ^{241}Am activity could be measured.

The final category concerns U-Zr particles, where the fuel has fused with the zircalloy cladding at high temperature, and should be the most stable in the environment. K001 (red) and R010 (dark green) are identified as containing Zr through EDS (see supplementary). K001 is the largest particle, and has a structure that varies between smooth and porous. As shown in fig. 7, the Zr is located only on the smooth parts, whereas the uranium is present in both smooth and porous parts. R010, one of the smallest particles, is smooth and contains Zr all over.

As maintained by Kashparov et al. [7], such surface analysis should be indicative of the chemical behaviour of the particles in the environment [7]. However, as pointed out by Konings et al., higher burnup will damage fuel structure through the diffusion of fission gases, which are released at lower temperatures with oxidized fuel [9]. Uranium isotope ratios will indicate the burnup of the particle, as will Cs ratios. Plutonium isotope ratios relate the particle specifically to RBMK type reactors. ^{137}Ba/^{138}Ba ratios will show to what degree Cs has diffused out of the particle, and while ^{85}Rb/^{87}Rb could show the retention of Kr fission gases, in these particles it will indicate the degree to which environmentally-derived Rb has covered the surface of the particle. Finally, ^{90}Sr/^{88}Sr as a function of burnup should not significantly change, allowing for an estimation of the time passed since particles were released from the reactor.

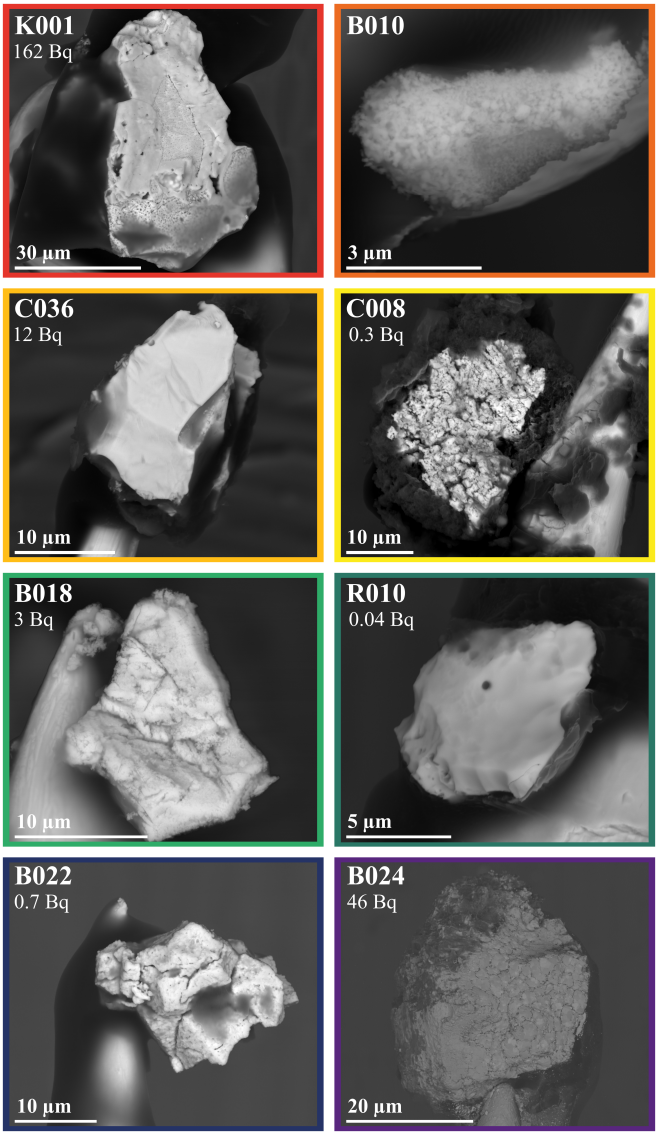

Figure 2: *Back scattered electron (BSE) images of eight particles from the CEZ, extracted via methods developed by Weiss and Leifermann [46], and labeled by origin (B: Pripyat, K: Kopachi, C: Cooling Pond, R: Red Forest). The total ^{137}Cs + ^{241}Am activity is given in Bq. For the rest of this paper, data points are colour coded to the specific particle.*

3.2 Actinides

Figure 3 compares measured actinide isotope ratios to known signatures from reactors. WWER and RBMK reactors operated in the former Soviet Union and largely continue to operate [34]. Both reactor types used fuels of varying ^{235}U enrichment, with WWERs at higher enrichment (e.g. 3.3, 3.6, 4.4 %) than RBMKs (e.g. 1.8, 2.0, 2.09 %). The particles measured by both rL-SNMS and LION align well with the known ratios for RBMK reactors, with the exception of B010, which does not contain plutonium.

Figure 3 shows that B010 is depleted uranium (DU), a by-product of the enrichment process with a ^{235}U/^{238}U ratio lower than natural uranium (0.007). However, it also contains measureable amounts of ^{236}U (Fig. 4), implying it derives from a reactor. This is consistent with Soviet-era fuel reprocessing, where U in spent fuel was separated and re-enriched [37, 54]. Because the B010 particle is the first DU

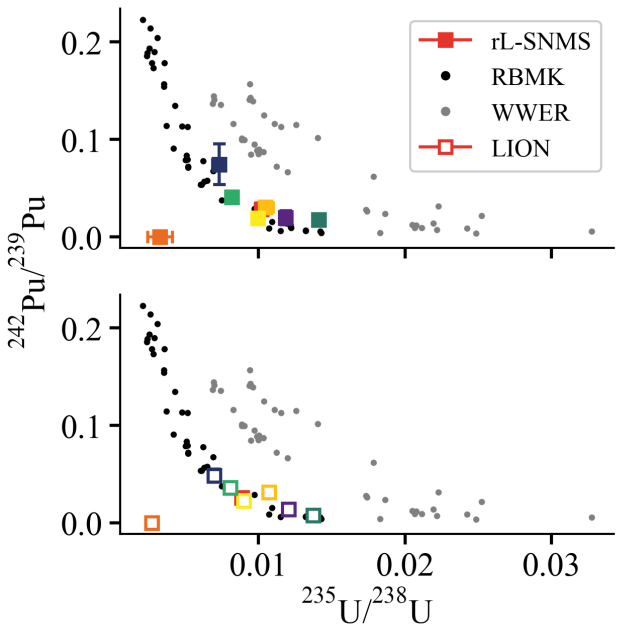

Figure 3: *Four-isotope plot showing the range in U and Pu isotope ratios depending on burnup. Ratios are compared to literature data on RBMK-type (black) and WWER-type (grey) reactors [37].*

particle reported in the CEZ, more of these particles would have to be analyzed to confirm whether this derives from ChNPP or from other civilian uses of DU.

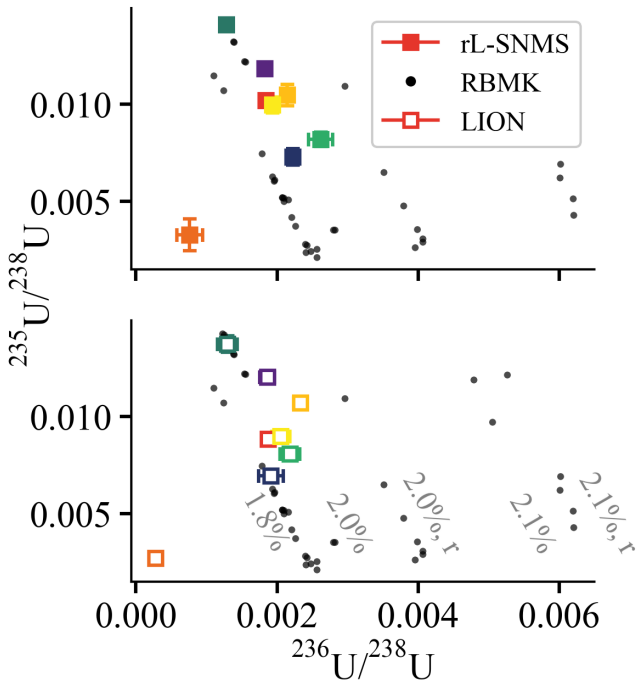

Figure 4: *Three-isotope plot for ^{235}U and ^{236}U normalised to ^{238}U. Ratios are compared to literature data on RBMK fuel assemblies [37] at known initial enrichment (noted in %). Some assemblies were made of recycled fuel (noted 'r'), enriched in ^{236}U.*

3.2.1 Capabilities of rL-SNMS and LION

An estimation of the initial fuel enrichment can be made by analysing ^{235}U vs ^{236}U, shown in figure 4. Previously published work shows that the fuel used in ChNPP was enriched to 2% [32], which was increased in later years to 2.4 % to increase safety [33]. Variations in ^{236}U/^{235}U can indicate fluctuations in neutron flux or energy at the microscopic level that may not have been captured in the gram-scale samples measured by Makarova et al. [37]. It should also be noted that sharp increases in burnup at the rim of a fuel pellet can result in significant variation in isotopic composition at the micrometer scale [3] [55].

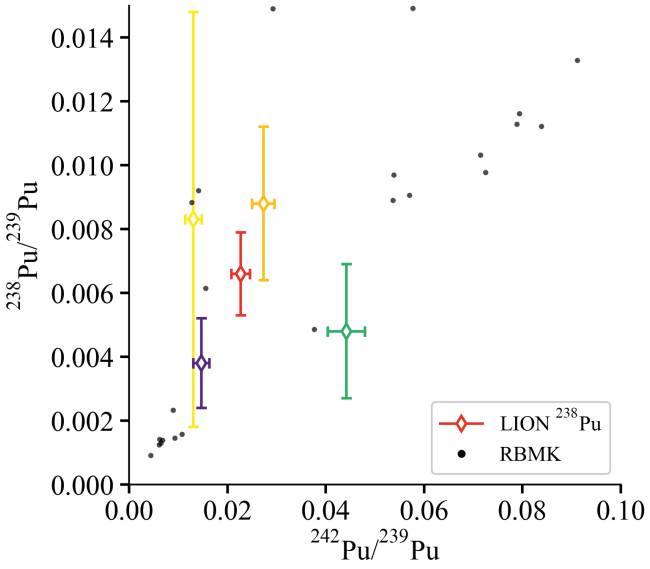

Figure 5: *Three-isotope plot for ^{238}Pu and ^{242}Pu normalised to ^{239}Pu compared to literature values for RBMKs as in earlier figures [37]. Two particles were not measureable above the limit of detection.*

As discussed in section 2.3, multi-element analysis does not sufficiently suppress ^{238}U interference on ^{238}Pu, as the non-resonant U signal is larger than the resonant Pu. The non-resonant signal can be subtracted by interleaving on- and off-resonance lasers every other shot (section 2.3). The ^{238}Pu/^{239}Pu ratio (Fig. 5) is an order of magnitude below that of ^{242}Pu, translating to extremely low signal and subsequently large errors, such that two particles (B022, R010) had errors over 100 % and are not shown. As previously noted in the literature [37], there should be an increasing trend with burnup, with significant variation possible [55], [3]. Though three of the five particles (C008, C036, K001) appear to deviate from the linear trend seen in Makarova, the data are within uncertainty of the previously published data and therefore cannot confidently say whether the samples derive from material that was subject to abnormal neutron conditions.

Reducing the uncertainty requires long and stable measurements of the particles, for which the mounting method is not suitable. Analysis length of the particles were limited because the desorption laser heated the glue attaching the particle to the needle, resulting in the loss of four particles (B022, B018, C008, R010).

Figure 6 shows deviations between the ^{240}Pu/^{239}Pu measured by rL-SNMS and LION. For the two U-Zr particles in particular, K001 (red) and R010 (dark green), the

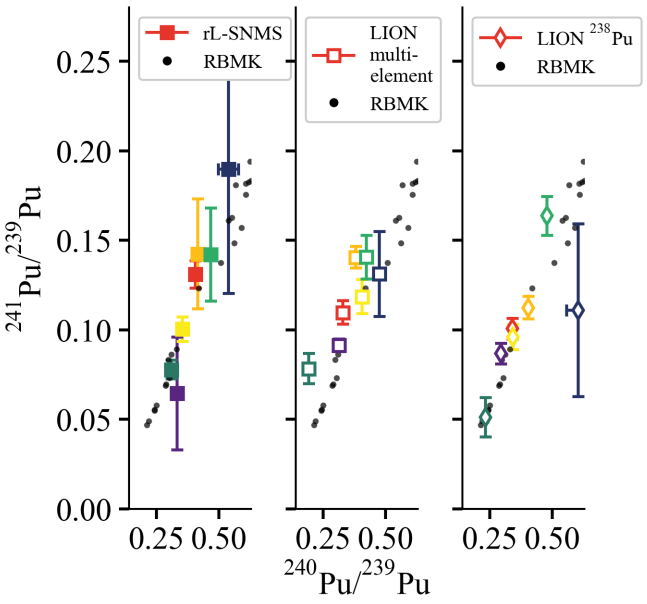

Figure 6: *Comparison of results from rL-SNMS, multi-element LION and ^{238}Pu blinked LION for the ratios ^{241}Pu/^{239}Pu and ^{240}Pu/^{239}Pu, with literature values for RBMKs [37]. All ^{241}Pu/^{239}Pu data is decay-corrected to the date of the Chornobyl accident, 26th April 1986.*

^{240}Pu/^{239}Pu values are notably higher when measured by rL-SNMS than by LION. We hypothesized that a compound may be overlapping at 240 m/z in the rL-SNMS, deriving from the zirconium area. Subsequent spatially resolved analyses by rL-SNMS targeted ^{240}Pu in the clearly identifiable regions with high and low Zr in K001. Results are shown in figure 7.

The first measurement in figure 7a was made in fast imaging mode, which increases the spatial resolution at the cost of signal intensity, but allows for a detailed map of the surface of the particle. Zirconium-rich areas form a hollow triangle shape on the particle, revealing a porous core of UO^+ in the middle and at the bottom edge. Fig. 7b shows that the resonant ^{240}Pu is not correlated to the Zr areas. The isotope ratios seen in figure 7c demonstrates the reproducibility of the rL-SNMS meaurements.

The measured ^{242}Pu/^{239}Pu and ^{236}U/^{238}U by rL-SNMS and LION are consistent within uncertainty (Fig. 7c). However, ^{240}Pu/^{239}Pu and ^{235}U/^{238}U values are measured higher in rL-SNMS than with LION, and are uncorrelated to the surface Zr content (Fig. 7b). A further statistical analysis comparing the performance of rL-SNMS and LION is found in the supplementary material. The noted discrepancies between ^{240}Pu/^{239}Pu and ^{235}U/^{238}U are not large enough to change the assessment of particle origin, evident by figure 3.

3.3 Fission Products

The fission products give insight into the environmental history of each individual particle since the accident, shown in Fig. 8. The ^{235}U/^{238}U ratio is used as a burnup monitor, where the lowest ratio has the highest burnup (particle B022). Measurement of Cs and Rb by SIMS on the LION could not be performed on K001 and R010 (U-Zr particles) due to poor quality spectra derived from interfering compounds. Measurements of Ba in B022, and ^{137}Cs γ in R010 were below the limit of detection and are not shown.

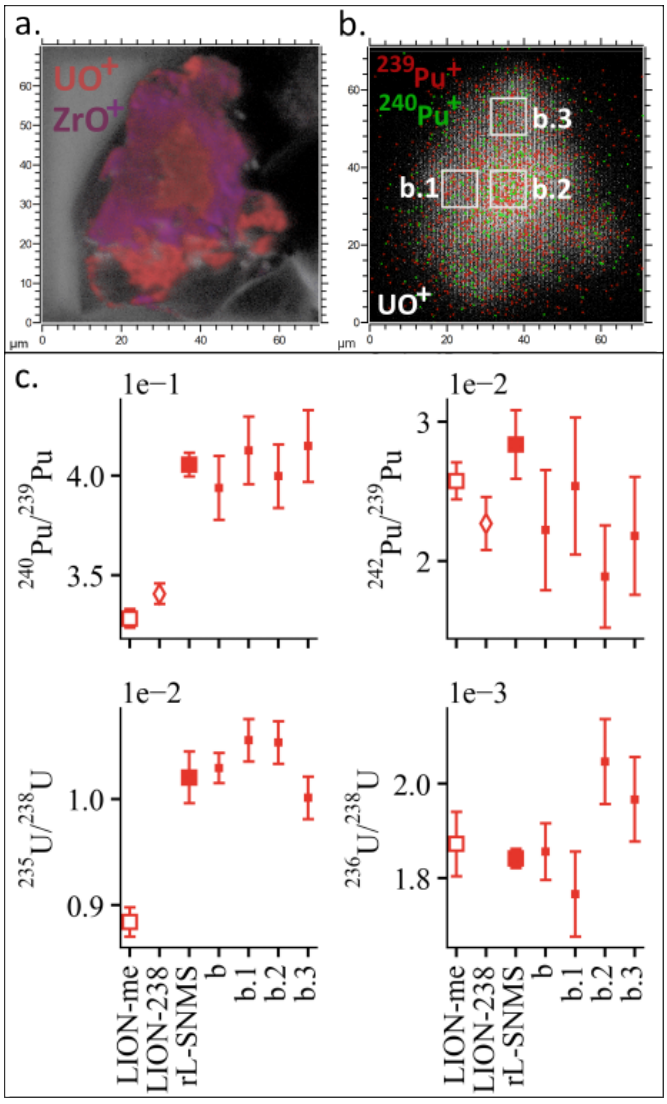

Figure 7: *a. Secondary ion fast imaging of K001, showing the concentration of UO^+ and ZrO^+ on the particle, overlayed on top of the total secondary ion image. b. rL-SNMS measurement of K001 resonant on plutonium, showing $^{239}Pu^+$ (red) $^{240}Pu^+$ (green) overlayed on UO^+ (white). Three 10 μm regions of interest (b.1, b.2, b.3) are selected to assess the isotope ratios in areas rich in Zr (b.1, b.3) versus without (b.2). c. Isotope ratios measured with the three methods in this work, and additional measurments done with rL-SNMS on the full particle (b), Zr-rich areas (b.1, b.3), and the center (b.2).*

3.3.1 Rb and Cs

The ratio predicted by web-KORIGEN++ (section 1.2.2) for ^{85}Rb/^{87}Rb derived from a thermal fission is in the range 0.41 to 0.53 (grey band in fig. 8a), where higher ratios would indicate more ^{85}Kr retention in the particle by completely decaying to ^{85}Rb. Only ^{85}Rb/^{87}Rb measured in particles B024 and B018 lie in this expected range, but at the high values of 0.55 ± 0.02 and 0.54 ± 0.01 respectively. We cannot correct for contamination with natural Rb (pink line) as both isotopes are naturally occurring, and therefore cannot interpret Kr retention in the particles. With the exception of B018, higher burnup particles show more environmentally-derived Rb.

The ^{137}Cs/^{135}Cs ratios in fig. 8b show an increasing trend with burnup, reflecting the local irradiation conditions of the

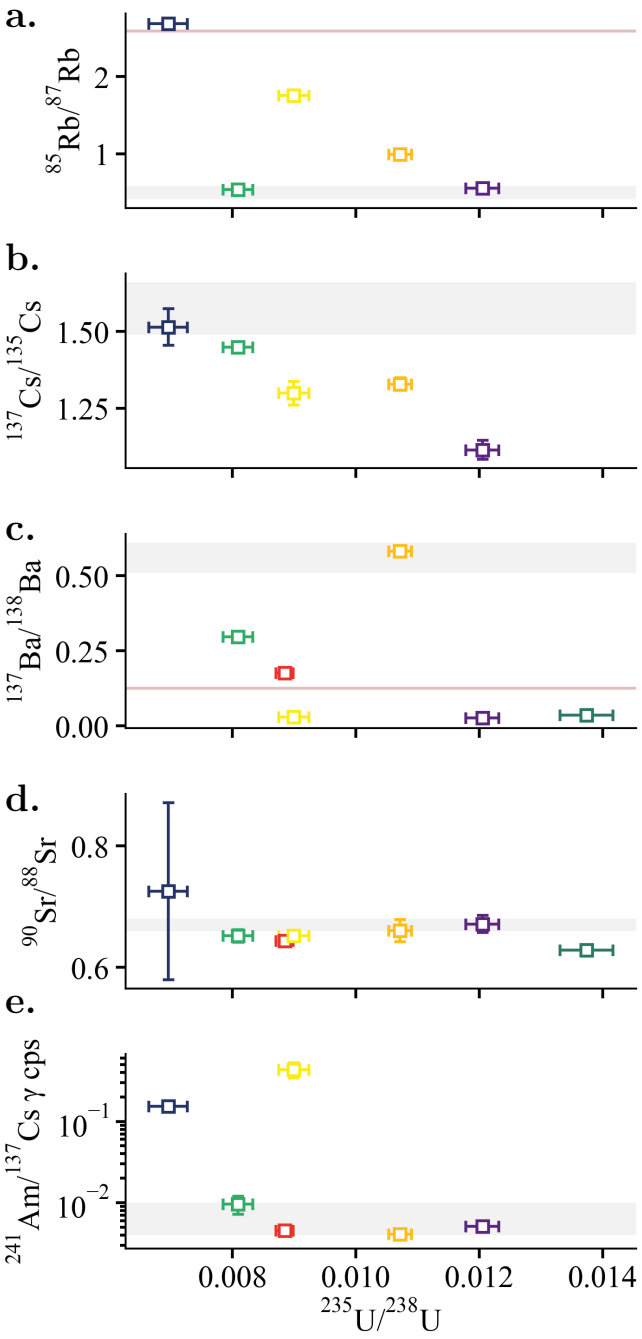

Figure 8: *Fission products as a function of $^{235}U/^{238}U$. Isotope ratios measured in LION via SIMS (Cs, Rb) and RIMS (Ba, Sr, corrected for contamination of naturally occurring isotopes, though Rb is not). Ratios are not date-corrected, but as measured in May 2022. Gamma spectrometry was done with a HPGe detector in coax geometry, comparing count rates at the 59.5 keV ^{241}Am peak and ^{137}Cs 661.7 keV peak. The naturally occurring ratios for Rb and Ba are indicated with a brown line. Estimated ranges, either from literature or in modelling, as described in the text, are in grey.*

fuel [20]. These ratios are significantly lower than the data previously reported for bulk soil samples from the CEZ [21] (dated to May 2022, shown in the grey band in figure 8), which likely represent an average across the reactor. This distinction may be particularly relevant if applied to Fukushima particles, where ambiguity remains as to whether particles were formed near the fuel, or in the volatile gases in the reactor [12, 21].

3.3.2 Sr, Ba, and gamma

The $^{90}Sr/^{88}Sr$ ratios in fig. 8c have an average ratio of 0.66 ± 0.02 (measured in May 2022) showing little variation with burnup within uncertainty. Using equation 2, this would indicate of 37 ± 1 years have passed since the particles were released from the reactor. The actual time of 36 years would result in a higher ratio (0.67 ± 0.01 shown in grey in figure 8). While the time passed since Chornobyl is well known, this ratio could act as a time stamp in cases where it is not. Such a method could be useful in categorizing particles of multiple independent releases, like the particles at Dounreay which were released into the environment over many years from different reactors [14].

The chemical behaviour of Cs has been measured in two ways. The $^{137}Ba/^{138}Ba$ ratio in fig. 8c shows a direct loss of Cs by the absence of ^{137}Ba accumulated outside the reactor. Comparison of $^{241}Am/^{137}Cs$ γ activity as shown in fig. 8e is a common measurement made by gamma spectrometry [14], presuming the chemical stability of parent nuclide ^{241}Pu, and the linear concentration increase of both nuclides with burnup (shown in fig. 6 for ^{241}Pu and in fig. 8 for ^{137}Cs).

After correction for environmentally-derived natural Ba (see supplementary), only C036 fully retains Cs in the particle, matching the expected reactor-derived ratio plus the ^{137}Cs decayed over 36 years (grey band fig. 8d). This is surprising as it is a cooling pond particle, indicating no leaching of any kind occurred when it was likely submerged for many years. Particles C008, B024 and R010 fall below the natural ratio (pink line fig. 8d) towards 0.03, the modelled ratio of $^{137}Ba/^{138}Ba$ directly out of the reactor without decay of ^{137}Cs. B018 and K001 have partially retained Cs. The supposed chemical stability of the U-Zr particles does not appear to translate to Cs retention in K001 and R010, and neither does particle burnup. Surface features in fig. 2 on the C008, B024 and K001 particles show physical ways by which Cs could have diffused out of the particle via pores and fractures, in contrast to the smoothness of C036.

In previous work on hot particles from a larger dataset, $^{241}Am/^{137}Cs$ γ ratios were measured in CEZ hot particles to be in the range 0.04 to 0.01 (grey band fig. 8e), where deviations by orders of magnitude are attributed to leaching behaviour in the environment [46]. In this interpretation, B018, K001, C036 and B024 fall within the predicted range, while B022 and C008 clearly deviate and show leaching behaviour. While ^{137}Cs γ was not measured above the limit of detection for R010, ^{241}Am γ was, indicating Cs leaching.

The differing behaviour of B024 is peculiar, as it indicates depletion of Cs with respect to Ba, but not with respect to Am. This could point to different time points at which the Cs is lost. Cesium loss can be attributed to the reactor operation, the extreme heat of the reactor meltdown, and/or subsequent loss in the environment (suddenly or gradually). Both ratios should therefore be considered in further study of leaching mechanisms.

4 Conclusions

RIMS analysis of both actinide and fission products offers a comprehensive study of isotope ratios in single hot particles from the Chornobyl Exclusion Zone. While many techniques may be used to measure a single attribute of a particle, this work shows how a range of isotope ratios can be used

to answer different questions useful to radioecology and nuclear forensics simultaneously. From the view of forensics, the actinide isotopes tie the sample to a specific nuclear reactor type, while Sr isotopes measure the time passed since release from the reactor. For radioecology, fission product isotopes can be measured alongside and distinguished from environmentally-derived isotopes. These ratios are influenced by fuel burnup, particle formation in the accident, and weathering in the environment. The results showed that unique isotope ratios can be measured for each particle, tied specifically to RBMK-type reactors in the mid 1980s, and that notable changes in the $^{137}Ba/^{138}Ba$ ratio indicate a range of retention of Cs in the particles.

Visual markers related to both fuel burnup and particle formation had more influence on Cs retention than burnup alone or sampling environment. The cooling pond particle C036 showed no leaching of Cs, making it the most environmentally stable particle in this data set, as predicted by its smooth surface. Highly porous structures as in particle C008 showed depletion in Cs with respect to Ba and Am, and B022 was leached with respect to Am. B024 and B018 showing visible fractures and pores typical of burnup structure, are significantly depleted of Cs compared to Ba, but not to Am. R010 and K001, both U-Zr particles, are leached of Cs with respect to Ba. R010 contains too little ^{137}Cs to be measured by gamma spectrometry, and K001 does not show any leaching behaviour with respect to Am. This suggests that a variety of Cs leaching pathways are possible, including no leaching at all. More particles will need to be analysed to establish a leaching mechanism dependent on both particle structure, burnup and environment.

Actinide ratios obtained by both rL-SNMS and LION were within the expected ratios for RBMK reactors at low to medium burnup. The most accurate and precise ratios are obtained with LION using a resonant three-step laser ionization scheme, with the addition of a fourth non-resonant laser to correct for non-resonant ionization of non-target elements. This is particularly important to measure the very low-abundance ^{238}Pu, which must be separated from the vastly dominant ^{238}U. The U-Zr particles K001 and R010 were distinguishable by lower than expected $^{240}Pu/^{239}Pu$ ratio measured by LION. Spatial analysis in rL-SNMS indicates that this is not caused by the presence of Zr or lack thereof, though further analysis is needed to determine the relevance of this discrepancy.

This work has demonstrated the versatile and flexible capabilities of multi-element RIMS analysis on single hot particles. Rather than a sacrificial final step, isotopic analysis can be performed quickly and in first order, preserving the particle for subsequent investigations such as leaching [46]. The increasing relationship between $^{137}Cs/^{135}Cs$ and burnup was observed, in a notably larger range than previously reported in the literature for samples from the CEZ. This highlights the need for single particle studies alongside bulk environmental analysis. The development of RIMS has diversified the range of elements that can be investigated non-destructively through the study of isotopic ratios, informed by their production pathways and sensitivity to environmental factors.

5 Acknowledgements

This Marie Sklodowska-Curie Action (MSCA) Innovative Training Network (ITN) receives funding from the European Union's H2020 Framework Programme under grant agreement no. 861198. Parts of this work was performed under the auspices of the U.S. Department of Energy by Lawrence Livermore National Laboratory under Contract DE-AC52-07NA27344, and was partially supported by the National Nuclear Security Agency Office of Defense Nuclear Nonproliferation Research and Development. LLNL-JRNL-844531. Additional thanks goes to Klaus Wendt and his group at Johannes Gutenberg University in Mainz for laser development and continued advice.

References

[1] Raiwa, M., Büchner, S., Kneip, N., Weiß, M., Hanemann, P., Fraatz, P., Heller, M., Bosco, H., Weber, F., Wendt, K., and Walther, C. *Spectrochimica Acta - Part B Atomic Spectroscopy* **190** 4 (2022).

[2] Bosco, H., Hamann, L., Kneip, N., Raiwa, M., Weiss, M., Wendt, K., and Walther, C. *Sci. Adv* **7** (2021).

[3] Savina, M. R., Isselhardt, B. H., and Trappitsch, R. *Analytical Chemistry* **93**, 9505–9512 7 (2021).

[4] Kuriny, V. D., Ivanov, Y. A., Kashparov, V. A., Loshchilov, N. A., Protsak, V. P., Yudin, E. B., Zhurba, M. A., and Parshakov, A. E. *Ann. Nucl. Energy* **20**, 415–420 (1993).

[5] Kashparov, V., Levchuk, S., Zhurba, M., Protsak, V., Beresford, N. A., and Chaplow, J. S. *Earth System Science Data* **12**, 1861–1875 8 (2020).

[6] Zheltonozhsky, V., Uck, K. M., and Bondarkov, M. *Journal of Environmental Radioactivity* **57**, 151–166 (2001).

[7] Kashparov, V. A. *Pollution Research, v.10 Special* , 21–30 (2003).

[8] Poudel, D., Avtandilashvili, M., Klumpp, J. A., Bertelli, L., and Tolmachev, S. Y. *Journal of Radiological Protection* **41**, 940–961 12 (2021).

[9] Konings, R. J., Wiss, T., and Beneš, O. *Nature Materials* **14**, 247–252 (2015).

[10] Kashparov, V. A., Ivanov, Y. A., Zvarisch, S. I., Protsak, V. P., Khomutinin, Y. V., Kurepin, A. D., and Pazukhin, E. M. *Nuclear Technology* **114**, 246–252 (1996).

[11] Salbu, B., Krekling, T., and Oughton, D. H. *The Analyst* **123**, 843–849 (1998).

[12] Morooka, K., Kurihara, E., Takehara, M., Takami, R., Fueda, K., Horie, K., Takehara, M., Yamasaki, S., Ohnuki, T., Grambow, B., Law, G. T., Ang, J. W., Bower, W. R., Parker, J., Ewing, R. C., and Utsunomiya, S. *Science of the Total Environment* **773** 6 (2021).

[13] Byrnes, I., Lind, O. C., Hansen, E. L., Janssens, K., and Salbu, B. *Science of the Total Environment* **727** 7 (2020).

[14] Particles Retrieval Advisory Group (Dounreay), S. E. P. A. S. (2012).

[15] Kristo, M. J., Gaffney, A. M., Marks, N., Knight, K., Cassata, W. S., and Hutcheon, I. D. *Annual Review of Earth and Planetary Sciences* **44**, 555–579 6 (2016).

[16] Mayer, K., Wallenius, M., and Varga, Z. *Chemical Reviews* **113**, 884–900 2 (2013).

[17] Betti, M., Tamborini, G., and Koch, L. *Analytical Chemistry* **71**, 2616–2622 (1999).

[18] Yamana, H., Yamamoto, T., and Moriyama, H. In *Plutonium in the environment - edited proceedings of the second invited international symposium,* Kudo, A., editor. Elsevier, (2001).

[19] Lantzos, I., Kouvalaki, C., and Nicolaou, G. *Progress in Nuclear Energy* **85**, 333–336 7 (2015).

[20] Robel, M., Isselhardt, B., Ramon, E., Hayes, A., Gaffney, A., Borg, L., Lindvall, R., Erickson, A., Carney, K., Battisti, T., Conant, A., Ade, B., Trellue, H., and Weber, C. *Journal of Environmental Radioactivity* **195**, 9–19 12 (2018).

[21] Zok, D., Blenke, T., Reinhard, S., Sprott, S., Kegler, F., Syrbe, L., Querfeld, R., Takagai, Y., Drozdov, V., Chyzhevskyi, I., Kirieiev, S., Schmidt, B., Adlassnig, W., Wallner, G., Dubchak, S., and Steinhauser, G. *Environmental Science and Technology* **55**, 4984–4991 4 (2021).

[22] Lakosi, L., Zsigrai, J., Kocsonya, A., Nguyen, T. C., Ramebäck, H., Parsons-Moss, T., Gharibyan, N., and Moody, K. *Journal of Radioanalytical and Nuclear Chemistry* **315**, 409–416 2 (2018).

[23] Querfeld, R., Schulz, W., Neubohn, J., and Steinhauser, G. *Journal of Radioanalytical and Nuclear Chemistry* **318**, 423–428 10 (2018).

[24] Fallon, C. M., Bower, W. R., Lyon, I. C., Livens, F. R., Thompson, P., Higginson, M., Collins, J., Heath, S. L., and Law, G. T. *ACS Omega* **5**, 296–303 1 (2020).

[25] Ambartzumian, R. V. and Letokhov, V. S. *Applied Optics* **11**, 354–358 (1972).

[26] Wendt, K., Trautmann, N., and Bushaw, B. A. *Nuclear Instruments and Methods in Physics Research B* **172**, 162–169 (2000).

[27] Savina, M. and Trappitsch, R. *Resonance Ionization Mass Spectrometry (RIMS): Fundamentals and Applications Including Secondary Neutral Mass Spectrometry*, 215–241. WILEY-VCH GmbH, 1 edition (2021).

[28] RILIS. `https://riliselements.web.cern.ch`.

[29] Kneip, N., Düllmann, C. E., Gadelshin, V., Heinke, R., Mokry, C., Raeder, S., Runke, J., Studer, D., Trautmann, N., Weber, F., and Wendt, K. *Hyperfine Interactions* **241** 12 (2020).

[30] Franzmann, M., Bosco, H., Walther, C., and Wendt, K. *International Journal of Mass Spectrometry* **423**, 27–32 12 (2017).

[31] Stephan, T., Trappitsch, R., Davis, A. M., Pellin, M. J., Rost, D., Savina, M. R., Yokochi, R., and Liu, N. *International Journal of Mass Spectrometry* **407**, 1–15 8 (2016).

[32] NRC, U. Technical report, US NRC, 1 (1987).

[33] IAEA. Technical report, IAEA, (1992).

[34] Devell, L., Guntay, S., and Powers, D. A. Technical report, OECD- NEA, 11 (1995).

[35] Šmaižys, A., Poškas, P., Narkunas, E., and Bartkus, G. *Nuclear Engineering and Design* **277**, 28–35 10 (2014).

[36] Plukiene, R., Plukis, A., Germanas, D., and Remeikis, V. *Lithuanian Journal of Physics* **49**, 461–469 (2009).

[37] Makarova, T. P., Bibichev, B. A., and Domkin, V. D. *Radiochemistry* **50**, 414–426 8 (2008).

[38] Desgranges, L., Pasquet, B., Valot, C., and Roure, I. *Journal of Nuclear Materials* **385**, 99–102 3 (2009).

[39] IAEA. `https://pris.iaea.org/pris/CountryStatistics/CountryDetails.aspx?current=UA`.

[40] Schulz, W., Gupta, D. K., Riebe, B., Steinhauser, G., and Walther, C. *Applied Geochemistry* **101**, 103–108 2 (2019).

[41] Mandel, M., Holtmann, L., Raiwa, M., Wunnenberg-Gust, A., Riebe, B., and Walther, C. *Journal of Hazardous Materials* **423** 2 (2022).

[42] Nucleonica. `https://nucleonica.com/Application/YieldsPlus.aspx`.

[43] Cort, M. D., Dubois, G., Fridman, S. D., Germanchuk, M. G., Izrael, Y. A., Janssens, A., Jones, A. R., Kelly, G. N., Kvasnikova, E. V., Matveenko, I., Nazarov, I. M., Pokumeiko, Y. M., Sitak, V. A., Stukin, E. D., Tabachny, L. Y., Tsaturov, Y. S., and Avdyushin, S. I. Technical report, European Commission, (1998).

[44] Willett, C. D., Kimmig, S. R., Cassata, W. S., Isselhardt, B. H., Liezers, M., Eiden, G. C., and Wacker, J. F. Technical report, LLNL, (2020).

[45] of Health, U. S. D. and Services, H. Technical report, Agency for Toxic Substances and Disease Registry, 4 (2004).

[46] Leifermann, L., Weiss, M., Chyzhevskyi, I., Dubchak, S., Fraatz, P., Hanemann, P., Raiwa, M., Schulz, W., Steinhauser, G., Weissenborn, T., and Walther, C. in press, (2023).

[47] PeakEasy. `https://peakeasy.lanl.gov/Home/About`.

[48] Grüning, C., Huber, G., Klopp, P., Kratz, J. V., Kunz, P., Passler, G., Trautmann, N., Waldek, A., and Wendt, K. *International Journal of Mass Spectrometry* **235**, 171–178 7 (2004).

[49] Stephan, T., Trappitsch, R., Davis, A. M., Pellin, M. J., Rost, D., Savina, M. R., Jadhav, M., Kelly, C. H., Gyngard, F., Hoppe, P., and Dauphas, N. *Geochimica et Cosmochimica Acta* **221**, 109–126 1 (2018).

[50] Hanemann, P., Bister, S., Raiwa, M., Reinhard, S., van Eerten, D., and Walther, C. *Journal of Radioanalytical and Nuclear Chemistry* (2022).

[51] Bosco, H., Weiss, M., Raiwa, M., Walther, C., Kneip, N., and Wendt, K. *Hyperfine Interactions* **241** 12 (2020).

[52] Fan, Q., Yamaguchi, N., Tanaka, M., Tsukada, H., and Takahashi, Y. *Journal of Environmental Radioactivity* **138**, 92–100 8 (2014).

[53] Poliakova, T., Weiss, M., Trigub, A., Yapaskurt, V., Zheltonozhskaya, M., Vlasova, I., Walther, C., and Kalmykov, S. in review, (2023).

[54] Betti, M. *Journal of Environmental Radioactivity* **64**, 113–119 (2003).

[55] Hanson, S. K. and Pollington, A. D. *Journal of Analytical Atomic Spectrometry* **36**, 1018–1027 5 (2021).